Structure and Energetics of Vinoxide and the X(^{2}A″) and A(^{2}A′) Vinoxy Radicals

Leah S. Alconcel, Hans-Jürgen Deyerl, Veysel Zengin, and Robert E. Continetti*

Department of Chemistry and Biochemistry, 0314, University of California—San Diego, 9500 Gilman Drive, La Jolla, California 92093-0314

Received: June 24, 1999; In Final Form: September 15, 1999

The photoelectron spectrum of vinoxide, $C_2H_3O^-$, at 355 nm is reported, showing photodetachment to both the X(^{2}A″) ground and first excited A(^{2}A′) states of the vinoxy radical. Both direct interpretations and Franck−Condon simulations of the photoelectron spectrum of this simple enolate anion have been used to obtain insights into the energetics and structures of the anion and the ground and first excited state of the neutral radical. Franck−Condon simulations were generated from ab initio geometry and frequency calculations using the CASSCF method and showed good agreement with the vibrational structure visible in the experimental spectrum. The electron affinity (E.A.$_{exp}$ = 1.795 ± 0.015 eV; E.A.$_{calc}$ = 1.82 eV) and separation energy of the ground and first excited states ($T_{0,exp}$ = 1.015 ± 0.015 eV; $T_{0,calc}$ = 0.92 eV) obtained from the ab initio calculations are in good accord with the experimental values.

1. Introduction

Enolate anions are intermediates in many organic reactions that involve carbon−carbon or carbon−oxygen bond formation. They also play a key role in the development of stereoselective and stereocontrolled syntheses of complex compounds.[1] Enolate radicals are important intermediates in combustion and photochemical smog cycles.[2] In particular, the vinoxy radical, $C_2H_3O^•$, is a major product of the reaction of odd oxygen and ethylene.[3] There is considerable interest in developing an understanding of the structures and energetics of these species.

The electron affinity of the vinoxy radical has been previously measured in both threshold photodetachment[4] and photoelectron spectroscopy experiments.[5] The photoelectron spectroscopy studies of vinoxide, $C_2H_3O^-$, reported to date have been carried out at lower photon energies, accessing only the ground X(^{2}A″) state of the vinoxy radical. Laser photodetachment of ground-state vinoxide anion X(^{1}A′) to the X(^{2}A″) state of the radical have established an electron affinity (E.A.) of 1.817 ± 0.023 eV.[5] Photodetachment and autodetachment studies have been used to characterize the structure of the ground and dipole-bound excited states of vinoxide (also called acetaldehyde enolate).[6,7] The ground- and dipole-bound excited-state anion geometries have also been computed using ab initio methods.[8]

The optically allowed B ← X transition of the vinoxy radical has been studied in considerable detail. Laser-induced fluorescence, infrared absorption, and photofragmentation studies have been used to study the vibrational structure of the ground X(^{2}A″) and second excited B(^{2}A″) states of the vinoxy radical.[2,3,9−14] The structure of the ground X(^{2}A″) state of the vinoxy radical has also been characterized experimentally using pure rotational spectra.[15] Dispersed fluorescence spectra have yielded frequencies of the normal vibrational modes for the B and X states.[3] Theoretical studies have included calculations of the structure and normal vibrational modes of both the B and X states using ab initio methods.[8,9,16−18] The B−X electronic transition has been modeled using multidimensional Franck−Condon factors obtained from the ab initio structures and force constants.[16]

In contrast, the first excited-state A(^{2}A′) of vinoxy has not been well-characterized previously. Hunziker *et al.* assigned a broad-band IR absorption to the A(^{2}A′) state and estimated the A−X electronic energy difference to be ≈1 eV.[19] Multiconfiguration Hartree−Fock calculations by Dupuis, Wendoloski, and Lester predicted that the A state would lie ≈0.5 eV above the ground state.[17] More recently, Yamaguchi carried out a CASSCF study on the X, A, B, and C states of vinoxy to gain insights into the fast nonradiative decay of the B(^{2}A″) state.[18] The calculated A−X electronic energy difference from Yamaguchi's study was 0.93 eV.[18]

One of the advantages of negative-ion photodetachment is the ability to access transitions to excited states of the radical that are optically forbidden from the ground-state radical. The transition from the ground X(^{2}A″) state of the vinoxy radical to the first excited A(^{2}A′) state is dipole-forbidden. This study reports photodetachment of vinoxide at 355 nm, providing structural and energetic information on both the ground and first excited states of the vinoxy radical. These experimental results are complemented by ab initio calculations on the anion and the radical. The transitions to the ground X(^{2}A″) state and first excited A(^{2}A′) state of the radical from the ground X(^{1}A′) state of the anion are both allowed and observed in photodetachment. The vibrational structure in the excited state is clearly resolved and is also visible, though not as clearly resolved, in the ground state. Franck−Condon factors (FCFs) for the vibronic transitions were calculated following the approach of Sharp and Rosenstock[20] and later generalized for polyatomic molecules by Warshel and Karplus.[21] More recently, Chen and co-workers[22] developed the specific method applied in this study for using ab initio structure and frequency results to calculate FCFs. The correspondence of the Franck−Condon simulations with the experimental photoelectron spectrum provides a benchmark for studies of the larger enolates and enolate radicals.

2. Experimental Section

The operation of the fast-ion-beam photoelectron spectrometer used in these experiments has been previously described in detail.[23] Room-temperature reagent-grade ethanol seeded in a

* Corresponding author. E-mail: rcontinetti@ucsd.edu.

10.1021/jp992126s CCC: $18.00
Published on Web 10/30/1999

10% mixture of N_2O in Ar produced vinoxide in a pulsed discharge ion source.[24] The mass-selected beam of vinoxide, $m/e = 43$, at an energy of 3 keV was crossed with the linearly polarized third harmonic (354.8 nm, 3.494 eV) of a Nd:YAG laser. The laboratory energy and recoil angle for each photoelectron is calculated from the time of flight and position of arrival recorded by the photoelectron detector. The electron kinetic energy in the center of the mass frame (eKE) is subsequently determined from this information, including correction of the electron velocity for the Doppler shift induced by the fast ion beam. The spectrometer was calibrated using photodetachment of $O^- \rightarrow O(^3P) + e^-$ and $NO^- \rightarrow NO(^2\Pi) + e^-$ at 355 nm. The photodetachment of O^- gives a peak at 2.032 eV that is reproduced with a maximum error of ±0.015 eV. The photodetachment of NO^- gives a vibrationally resolved photoelectron spectrum with peaks belonging to the NO^- ($v'' = 0$) to NO ($v' = 0-5$) progression which are reproduced with a maximum error of ±0.015 eV.[25]

3. Ab Initio Calculations

The energetics, structures, harmonic frequencies, and force constants for vinoxide and the vinoxy radicals were calculated to aid in the interpretation of the experimental photoelectron spectrum. High-level ab initio computations are presumed to be essential because of involvement of the anion and the open-shell low-lying excited state. The structures of vinoxide and the ground- and excited-state vinoxy radical were optimized at the CASSCF level. To justify the necessity for using such a high level of theory, a UMP2 calculation was performed on the ground state of the radical to examine the effects of spin contamination. The desired $\langle S^2 \rangle$ for a doublet state is 0.75, and the $\langle S^2 \rangle$ obtained at the UMP2 level was 0.873. A single-reference wave function is therefore inappropriate for computing the vinoxy radical structure. In addition, calculating the first excited-state structure requires the inclusion of configuration interaction with multiple excitations. To maintain consistency, the vinoxide and vinoxy radicals were all calculated at the CASSCF level of theory using the DALTON program package.[26]

The four orbitals which were chosen for the active space were, in order of increasing energy, the bonding CCO π(a″) orbital, the oxygen σ_{2px}(a′) orbital, and the nonbonding and antibonding CCO π(a″) orbitals. In accordance with previous studies, C_s symmetry was imposed on the geometries of the anion and radicals.,[9,16,17,27] The Pople valence triple-ζ basis set[28] including diffuse and polarization functions (6-311++G**) was used in DALTON to perform the geometry optimizations and vibrational analysis. The diffuse functions are required to correctly compute the absolute energy of the anion.[29] The frequencies of the normal vibrational modes were scaled by a factor of 0.91 before use in the Franck−Condon factor calculations. This scaling factor has been determined to be appropriate for calculations using Pople's triple-ζ basis sets on molecules with up to three heavy atoms.[30] Gaussian 94[31] was used to include dynamic correlation in the absolute energies because the DALTON program does not have the capability to perform single-point CASSCF-MP2[32] calculations on the CASSCF optimized geometries.

4. Franck−Condon Factor Calculations

The intensity of a transition between vibrational modes of two different electronic states can be expressed as the square of the overlap integral between the vibrational wave functions.[21]

$$I(m,n) = [\int \Psi_m^M(Q^M)\Psi_n^N(Q^N)\, dQ^M]^2$$

Here, m and n represent the number of quanta in the electronic states M and N and the Q's represent the nuclear displacement coordinates from the equilibrium geometry. The Franck−Condon factors (FCFs) were evaluated using the generating function method for a multidimensional harmonic oscillator, neglecting anharmonic effects.[21] The parallel mode approximation, in which it is assumed that the ground-state anion and the neutral share normal coordinates, is often inappropriate for polyatomic molecules. Mode mixing induced by changes in geometry and the form of the normal modes between the ground-state anion and the neutral species, called the Duchinsky effect,[20] must be taken into account. The Duchinsky effect is handled by a conversion of the coordinates of the anion into the coordinates of the neutral radical as given in the following equation:

$$\mathbf{Q}' = \mathbf{JQ} + \mathbf{K}$$

The matrix **J** and the vector **K** define the transformation and the matrices **Q** and **Q′** represent the normal coordinates of the anion and the ground-state neutral species, respectively.

The algorithm used to implement the generating function method for calculating Franck−Condon factors including the Duchinsky effect was developed by Chen and co-workers.[22] Chen's FCF code generates simulated photoelectron spectra using the Cartesian coordinates, normal vibrational modes, frequencies, and reduced masses from Gaussian 94 geometry optimizations and frequency calculations. The substitution of DALTON output for Gaussian 94 is straightforward. The details of the calculation can be found in ref 22. Transforming the calculated transition energy into the electron kinetic energy yielded stick spectra that were convoluted with a Gaussian function in which the full-width half-maximum was varied to simulate the resolution ($\Delta E_{fwhm}/E \sim 4\%$) in the experimental photoelectron spectrum. Because no hot bands were observed in the experimental spectrum, the anion temperature was assumed to be 0 K.

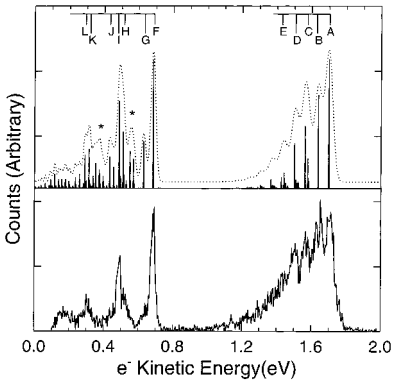

Figure 1. Experimental and simulated photoelectron spectra of vinoxide at 355 nm. Peak labels indicate transitions in the simulated spectrum corresponding to features in the experimental spectrum and are specified in Tables 5 and 6. As noted in the text, the vibrational frequencies are scaled prior to simulating the spectra. The peaks marked by the asterisks in the simulation of the A(^{2}A′) excited state were not observed experimentally.

5. Results and Discussion

The photoelectron spectrum of vinoxide at 355 nm is shown in Figure 1. First, the electron affinity and separation energy

TABLE 1: Calculated Structures of Vinoxide and the Vinoxy Radicals[a]

	X(^{1}A′)		X(^{2}A″)		A(^{2}A′)
	theor.	exp.	theor.	exp.	theor.
C_1-C_2	1.384	1.324[a]	1.439	1.398[b]	1.334
C_2-O	1.246	1.334[a]	1.217	1.268[b]	1.341
C_1-H_1	1.080		1.074		1.074
C_1-H_2	1.078		1.074		1.072
C_2-H_3	1.109		1.090		1.077
$\angle C_1C_2O$	130.4	129.4[a]	122.9	122.2[b]	124.6
$\angle C_1C_2H_3$	113.3		117.5		124.2
$\angle H_1C_1C_2$	121.5		119.6		122.0
$\angle H_2C_1C_2$	119.8		120.8		119.4

[a] Calculated using the CASSCF method and the 6-311++G** basis set; atom labels are in Figure 2, bond lengths given in angstroms, and angles in degrees. [b] Reference 6, with ±0.019 Å and ±0.025° uncertainties. [c] Reference 15.

between $v' = 0$ of the ground and excited states of the neutral species were determined directly from the experimental photoelectron spectrum. Vinoxide undergoes photodetachment to both the ground and first excited states of the neutral radical. When vinoxide is photodetached to the ground X(^{2}A″) state of the vinoxy radical, an electron is ejected from the HOMO (the CCO nonbonding π(a″) orbital), leaving the orbital singly occupied. This configuration is commonly called the formyloxy radical ($^{\bullet}CH_2-CH{=}O$). During photodetachment to the first excited state of the vinoxy radical, an electron is ejected from the oxygen σ_{2px}(a′) orbital, leaving it singly occupied. The resulting configuration is commonly called the vinyloxy radical ($CH_2{=}CH-O^{\bullet}$). The values for E.A. (1.795 ± 0.015 eV) and T_0 (1.015 ± 0.015 eV) from this experiment are in good agreement with values obtained experimentally by Lineberger[5] (E.A. = 1.817 ± 0.023 eV) and Hunziker[19] ($T_0 \sim 1$ eV).

Examination of the results of the ab initio calculations can aid in the interpretation of the photoelectron spectra. The bond lengths and angles obtained from the DALTON optimizations using the CASSCF method and the 6-311++G** basis set for vinoxide and the neutral radicals are listed in Table 1. Previous experimental values are included for ground-state vinoxide and vinoxy.[6,15] The major changes between the anion and the two neutral geometries are centered on the CC and CO bonds and the CCO bond angle. Table 2 compares the scaled results from the normal mode calculations with experimentally determined frequencies.[3,6,7] The normal modes near 3000 cm^{-1} with a′ symmetry correspond to the CH stretches in the molecule. The succeeding six modes with a′ symmetry correspond to the other in-plane vibrations. The three modes with a″ symmetry correspond to out-of-plane bends. The modes for the X(^{2}A″) state are in order $\nu_1-\nu_{12}$ as designated by Brock and Rohlfing[3] with the exception of modes ν_7 and ν_8. The interchange is supported by the experimental data in this study and the correspondence of the Cartesian displacements calculated for ν_7 with the CC stretch and those calculated in this study for ν_8 with the $C_1H_1H_2$ rock. Because the modes for the X(^{1}A′) state of the anion are similar to those for the X(^{2}A″) state of the radical, they have been arranged correspondingly. The same numbering scheme is not applicable to the A(^{2}A′) state because the Cartesian displacements of the vibrational modes differ from those of the X(^{2}A″) state. The a′ (in-plane) vibrational mode types for the A(^{2}A′) state have been identified and labeled in Table 2. The CC stretch and CO stretch frequencies are nearly reversed from the X(^{2}A″) state to the A(^{2}A′) state, which is consistent with the predicted changes in the CC and CO bond lengths from the formyloxy to the vinyloxy configuration of the radical.

The absolute energies in Table 3 were obtained from CASSCF calculations of vinoxide and vinoxy radicals at their optimized geometries and corrected by adding the zero-point energies. The relative anion and ground-state radical energy corresponds to the adiabatic electron affinity and is in good agreement (ΔE < 0.1 eV) with the experimental value after the CASSCF-MP2 correction (Table 4), as is the separation energy between the ground and excited states of the radical, T_0.

The simulated spectrum is plotted above the experimental spectrum in Figure 1. Only six of the vibrational modes corresponding to the in-plane vibrations were included in the FCF calculations. The three out-of-plane bending modes are not expected to contribute to the spectrum by symmetry. Vibronic interactions in the X(^{2}A″) state that may make these modes active have been neglected. Features due to the ≈3000-cm^{-1} vibrational modes would appear at low eKE in the experimental spectrum, but there is little evidence for participation of these modes in the spectra and they have been neglected because of computational time constraints. The major features in the simulated spectrum can be assigned to specific vibrational transitions, as shown in Tables 5 and 6. In the transition from the ground-state anion to the ground state of the neutral radical, the two normal vibrational modes of the radical that produce high-intensity Franck−Condon overlap are the CC stretching mode and the CCO bending mode, shown in Figure 2. These have been designated as the ν_7 and ν_9 modes respectively in previous studies.[3,9,16] The spacing between peaks A and C yields a value of 1100 ± 120 cm^{-1} for ν_7, which provides support for interchanging the mode numbers of the CC stretch and the $C_1H_1H_2$ rock from that adopted by Brock and Rohlfing.[3]

TABLE 2: Scaled Frequencies of Normal Vibrational Modes (in cm^{-1}) for Vinoxide and the Vinoxy Radicals[a]

	X(^{1}A′)		X(^{2}A″)			A(^{2}A′)	
vibration	theor.	exp.	theor.	exp.	vibration	theor.	exp.
ν_1, CH asym. str., a′	3013		3110		ν_1, CH asym. str., a′	3095	
ν_2, CH sym. str., a′	2852		3004		ν_2, CH stretch, a′	3025	
ν_3, CH stretch, a′	2660		2890		ν_3, CH sym. str., a′	3005	
ν_4, CO stretch, a′	1568		1525	1543[c]	ν_4, CC stretch, a′	1590	1580[d]
ν_5, CHH scissors, a′	1425		1441	1486[c]	ν_5, CHH scissors, a′	1403	1350[d]
ν_6, OCH bend, a′	1340		1373	1366[c]	ν_6, OCH bend, a′	1258	
ν_7, CC stretch, a′	1179		1101	957[c]	ν_7, CO stretch, a′	1083	
ν_8, CHH rock, a′	976		934	1143[c]	ν_8, CHH rock, a′	929	
ν_9, CCO bend, a′	519	526[a]	489	500[c]	ν_9, CCO bend, a′	441	460[d]
ν_{10}, OCH wag, a″	966		892	703[c]	a″	847	
ν_{11}, CHH wag, a″	420	375[b]	599	557[c]	a″	627	
ν_{12}, torsion, a″	643		406	404[c]	a″	180	

[a] Calculated using the CASSCF method and the 6-311++G** basis set; a′ and a″ indicate the C_s symmetry of the vibrational modes. [b] Reference 7. [c] Reference 6. [d] Reference 3. [e] This work, with ±120 cm^{-1} uncertainties.

TABLE 3: Absolute CASSCF and CASSCF-MP2 Energies (in hartrees)[a]

species	CASSCF	CASSCF-MP2
X(^{1}A′)	−152.328 323 8	−152.841 895 8
X(^{2}A″)	−152.323 047 0	−152.774 893 0
A(^{2}A′)	−152.291 209 6	−152.741 016 3

[a] With 6 or 5 electrons, respectively, in 4 orbitals and the 6-311++G** basis set. Corrected by zero point energies.

TABLE 4: Relative CASSCF and CASSCF-MP2 Energies (in eV)[a]

	CASSCF	CASSCF-MP2
E.A.	0.14	1.82
T_0	0.87	0.92

[a] With 6 or 5 electrons, respectively, in 4 orbitals and the 6-311++G** basis set.

TABLE 5: Position along Energy Axis (eKE) (in eV) and Quanta of Vibrational Modes of Transitions to Ground-State Vinoxy Radical in Simulated Photoelectron Spectrum[a]

	X(^{2}A″)			
X(^{1}A′), all modes	489 cm^{-1}: CCO bend	1101 cm^{-1}: CC stretch	eKE	peak label
$v''=0$	$v'=0$	$v'=0$	1.699	A
$v''=0$	$v'=1$	$v'=0$	1.638	B
$v''=0$	$v'=2$	$v'=0$	1.578	C
$v''=0$	$v'=0$	$v'=1$	1.562	C
$v''=0$	$v'=1$	$v'=1$	1.502	D
$v''=0$	$v'=2$	$v'=1$	1.441	E
$v''=0$	$v'=0$	$v'=2$	1.426	E

[a] Frequencies have been scaled.

TABLE 6: Position along Energy Axis (eKE) (in eV) and Quanta of Vibrational Modes of Transitions to Excited-State Vinoxy Radical in Simulated Photoelectron Spectrum[a]

	A(^{2}A′)				
X(^{1}A′) all modes	441 cm^{-1}: CCO bend	1403 cm^{-1}: CH_2 scissors	1590 cm^{-1}: CC stretch	eKE	peak label
$v''=0$	$v'=0$	$v'=0$	$v'=0$	0.684	F
$v''=0$	$v'=1$	$v'=0$	$v'=0$	0.629	G
$v''=0$	$v'=0$	$v'=1$	$v'=0$	0.510	H
$v''=0$	$v'=0$	$v'=0$	$v'=1$	0.487	I
$v''=0$	$v'=1$	$v'=0$	$v'=1$	0.432	J
$v''=0$	$v'=0$	$v'=1$	$v'=1$	0.313	K
$v''=0$	$v'=0$	$v'=0$	$v'=2$	0.290	L

[a] Frequencies have been scaled.

Similarly, spacing in the experimental spectrum between the peaks labeled A and B in the simulated spectrum yielded a value of 460 ± 120 cm^{-1} for ν_9. Both quantities are consistent with peak spacings measured by Lineberger and co-workers, who found the A−B peak spacing to be 450 cm^{-1} and the B−C peak spacing to be 550 cm^{-1}.[5] Because the major geometrical changes from vinoxide to ground-state vinoxy consist of a contraction of the CCO bond angle, an increase in the CC bond length and a decrease in the CO bond length, it is reasonable that these modes would be active during the transition.

Three vibrational modes of the excited-state radical produce intense FCF overlap in the simulation. These are the CCO bending mode, the CH_2 scissoring mode, and the CC stretching mode, each of which is illustrated in Figure 2. The CH_2 scissoring mode also includes some stretching of the CO bond. As in the transition to the ground-state radical, when the geometrical changes from vinoxide to excited-state vinoxy are considered, it is reasonable that these modes would be active. The spacings between the peak in the experimental spectrum

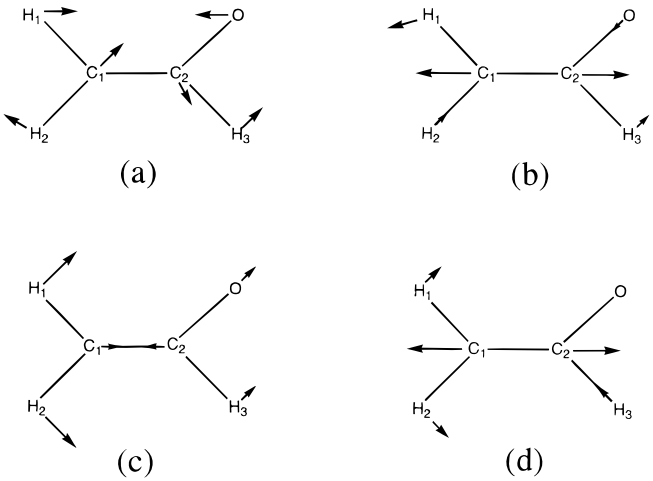

Figure 2. Calculated vibrational modes of the ground and first excited state of vinoxy labeled as follows: (a) CCO bending mode of ground and excited states, (b) CC stretching mode of ground state, (c) CH_2 scissoring mode of excited state, and (d) CC stretching mode of excited state.

labeled as F in the simulated spectrum and those labeled as G, H, and I correspond to $v'=1$ in the CCO bend, the CH_2 scissors, and the CC stretch. These experimental values $\nu_9 = 460 \pm 120$ cm^{-1}, $\nu_5 = 1350 \pm 120$ cm^{-1}, and $\nu_4 = 1580 \pm 120$ cm^{-1} are shown in Table 2 and constitute the first reported measurements of these frequencies. They agree well with the scaled frequencies calculated in this study, also reported in Table 2.

The vibrational mode that consists predominantly of CO stretching produces some Franck−Condon overlap in the simulated excited-state spectrum, which seems logical because the calculated CO bond length changes by 0.1 Å from the X(^{1}A′) state of vinoxide to the A(^{2}A′) state of the radical. However, the A(^{2}A′) ← X(^{1}A′) transition region in the experimental spectrum does not show the excitation of the CO stretching and $C_1H_1H_2$ rocking modes that appears in the simulation. The major features resulting from these excitations are marked with asterisks in the simulation in Figure 1. Overall, the simulation shows greater vibrational excitation in the A(^{2}A′) state than that observed experimentally. The lack of a progression in the CO stretching mode may be explained by significant off-diagonal overlap between the CH_2 scissoring mode (ν_5) and the CO stretching mode (ν_7) present in the Duchinsky rotation. As noted above, ν_5 does include some CO stretching motion. The general overestimation of the vibrational excitation presumably arises because of the difficulty in correctly modeling excited states using ab initio methods. Use of a correlation-consistent basis set or a multireference configuration interaction calculation would be expected to give more precise force constants and geometries for the excited state; however, this was beyond the scope of the present study.

The structures calculated here can be compared to previous theoretical and experimental studies. The structural information computed for the ground-state vinoxy radical in the current study is in agreement with previous computational[8,9,16−18] efforts. The recent computational results of Yamaguchi[18] for the first excited-state vinoxy radical structure also agree with the structure obtained in this study. However, previously obtained experimental geometries for vinoxide and ground-state vinoxy show consistent disagreement with the ab initio structures (Table 1). Lineberger and co-workers obtained a CO bond length of 1.334 ± 0.019 Å for ground-state vinoxide from analysis of rotationally resolved autodetachment spectra.[6] In the theoretical calculations reported here, the CO bond optimized to 1.246 Å, which

is characteristic of a double bond. The calculated CC bond length of 1.384 Å is significantly longer than the experimental bond length of 1.324 Å for vinoxide.[6] A comparison of the experimental and theoretical values for the CO and CC bond lengths of the ground-state vinoxy radical yields a similar trend. The CASSCF calculations underestimate the CO bond by 3−4% and overestimate the CC bond by 4−7%. The calculated CCO bond angles for vinoxide and ground-state vinoxy deviate less than 1% from the experimental values. Extrapolation of these trends to the A(^{2}A′) excited state suggests that the actual CO and CC bond lengths may be nearer 1.42 and 1.29 Å, respectively. These bond lengths are more consistent with the vinyloxy configuration predicted for photodetachment from the oxygen σ_{2px}(a′) orbital. If this is correct, it may indicate that the consistency of the errors in the calculated bond lengths for the structures of vinoxide and both of the vinoxy radicals leads to the reasonable Franck−Condon simulations of the spectra. However, the absence of a progression in the CO stretch following photodetachment to the A(^{2}A′) excited state suggests that the calculated CO bond length of 1.341 Å, which is similar to the experimental CO bond length in the ground state of the anion, 1.334 Å, is not unreasonable. Confirmation of the A(^{2}A′) excited-state structure will require higher level ab initio calculations.

6. Conclusion

This study reports the 355 nm photoelectron spectrum of vinoxide, showing photodetachment to both the ground and first excited state of the vinoxy radical. Ab initio calculations on vinoxide and the two lowest electronic states of vinoxy were carried out to aid in the interpretation of the observed vibronic structure. The theoretical and experimental energetics of this system are in agreement. The positions and intensities of vibronic transitions from vinoxide to the ground- and excited-state vinoxy radical observed in the photoelectron spectrum of vinoxide are simulated using polyatomic FCF calculations. Good agreement was found between the experimental and simulated photoelectron spectra reported here, despite discrepancies between the calculated structures and previous experimental results. The comparison to the photoelectron spectra presented here provides the first reported experimental characterization of the lowest excited state of the vinoxy radical.

In future work, the evolution of the vibronic structures of the three- and four-carbon enolate radicals will be studied. Photodetachment studies have been performed on these species and the ground and first excited states have both been observed. The transition from the ground to the first excited state is optically forbidden for the larger enolates as well as vinoxy. Similarities between the experimental photoelectron spectra at 355 nm of vinoxy and the three- and four-carbon enolates make it plausible that, to a large extent, the same modes are active in the larger enolates. A thorough study of enolates of varying sizes and substitutions may provide further insights into the similarities of reaction pathways involving this important class of organic compounds.

Acknowledgment. This work was supported by the Chemistry Division of the National Science Foundation under Grant CHE 97-00142. R.E.C. is a Camille Dreyfus Teacher-Scholar, an Alfred P. Sloan Research Fellow, and a Packard Fellow in Science and Engineering. L.S.A. is supported by a Cota Robles Fellowship. H.J.D. gratefully acknowledges partial support from a Forschungstipendium sponsored by the Deutsche Forschungsgemeinschaft and DOE Grant DE-FG03-98ER14879. We thank Drs. Peter Taylor and B. Joakim Persson for helpful discussions concerning ab initio methods.

References and Notes

(1) Ager, D. J.; East, M. B. *Asymmetric Synthetic Methodology*; CRC Press: Boca Raton, 1996; pp 97−122.

(2) Wan, R.; Chen, X.; Wu, F.; Weiner, B. R. *Chem. Phys. Lett*. **1996**, *260*, 539.

(3) Brock, L. R.; Rohlfing, E. A. *J. Chem. Phys*. **1997**, *106*, 10048.

(4) Jackson, R. L.; Hiberty, P. C.; Brauman, J. I. *J. Chem. Phys*. **1981**, *74*, 3705.

(5) Ellison, G. B.; Engelking, P. C.; Lineberger, W. C. *J. Phys. Chem*. **1982**, *86*, 4873.

(6) Mead, R. D.; Lykke, K. R.; Lineberger, W. C.; Marks, J.; Brauman, J. I. *J. Chem. Phys*. **1984**, *81*, 4883.

(7) Mullin, A. S.; Murray, K. K.; Schulz, C. P.; Szaflarski, D. M.; Lineberger, W. C. *J. Chem. Phys*. **1992**, *166*, 207.

(8) Wetmore, R. W.; Schaefer, H. F., III; Hiberty, P. C.; Brauman, J. I. *J. Am. Chem. Soc*. **1980**, *102*, 5470.

(9) Osborn, D. L.; Choi, H.; Mordaunt, D. H.; Bise, R. T.; Neumark, D. M.; Rohlfing, C. M. *J. Chem. Phys*. **1997**, *106*, 3049.

(10) Inoue, G.; Akimoto, H. *J. Chem. Phys*. **1981**, *74*, 425.

(11) Kleinermanns, K.; Luntz, A. C. *J. Phys. Chem*. **1981**, *85*, 1966.

(12) Jacox, M. E. *Chem. Phys*. **1982**, *69*, 407.

(13) DiMauro, L. F.; Heaven, M.; Miller, T. A. *J. Chem. Phys*. **1984**, *81*, 2339.

(14) Barnhard, K. I.; He, M.; Weiner, B. R. *J. Phys. Chem*. **1996**, *100*, 2784.

(15) Endo, Y.; Saito, S.; Hirota, E. *J. Chem. Phys*. **1985**, *83*, 2026.

(16) Yamaguchi, M.; Momose, T.; Shida, T. *J. Chem. Phys*. **1990**, *93*, 4211.

(17) Dupuis, M.; Wendoloski, J. J.; Lester, W. A., Jr. *J. Chem. Phys*. **1982**, *76*, 488.

(18) Yamaguchi, M. *Chem. Phys. Lett*. **1994**, *221*, 531.

(19) Hunziker, H. E.; Kneppe, H.; Wendt, H. R. *J. Photochem*. **1981**, *17*, 377.

(20) Sharp, T. E.; Rosenstock, H. M. *J. Chem. Phys*. **1964**, *41*, 3453.

(21) Warshel, A.; Karplus, M. *Chem. Phys. Lett*. **1972**, *17*, 7.

(22) Chen, P. In *Unimolecular and Bimolecular Reaction Dynamics*; Ng, C. Y., Baer, T., Powis, I., Eds.; Wiley & Sons: Chichester, 1994; pp 371−425.

(23) Zengin, V.; Persson, B. J.; Strong, K. M.; Continetti, R. E. *J. Chem. Phys*. **1996**, *105*, 9740.

(24) Osborn, D. L.; Leahy, D. J.; Cyr, D. R.; Neumark, D. M. *J. Chem. Phys*. **1996**, *104*, 5026.

(25) Siegel, M. W.; Celotta, R. J.; Hall, J. L.; Levine, J.; Bennett, R. A. *Phys. Rev. A* **1972**, *6*, 607.

(26) Helgaker, T.; Jensen, H. J. Aa.; Jørgensen, P.; Olsen, J.; Ruud, K.; Gren, H.; Andersen, T.; Bak, K. L.; Bakken, V.; Christiansen, O.; Dahle, P.; Dalskov, E. K.; Enevoldsen, T.; Fernandez, B.; Heiberg, H.; Hettema, H.; Jonsson, D.; Kirpekar, S.; Kobayashi, R.; Koch, H.; Mikkelsen, K. V.; Norman, P.; Packer, M. J.; Saue, T.; Taylor, P. R.; Vahtras, O. *DALTON*, An Electronic Structure Program, Release 1.0, 1997.

(27) Persson, B. J.; Taylor, P. R., unpublished.

(28) Krishnan, R.; Binkley, J.; Seeger, R.; Pople, J. A. *J. Chem. Phys*. **1980**, *72*, 650.

(29) Clark, T.; Chandrasekhar, J.; Spitznagel, G. W.; Schleyer, P. v. R. *J. Comput. Chem*. **1983**, *4*, 294.

(30) Scott, A. P.; Radom, L. *J. Phys. Chem*. **1996**, *100*, 16502.

(31) Frisch, M. J.; Trucks, G. W.; Schlegel, H. B.; Gill, P. M. W.; Johnson, B. G.; Robb, M. A.; Cheeseman, J. R.; Keith, T.; Petersson, G. A.; Montgomery, J. A.; Raghavachari, K.; Al-Laham, M. A.; Zakrzewski, V. G.; Ortiz, J. V.; Foresman, J. B.; Cioslowski, J.; Stefanov, B. B.; Nanayakkara, A.; Challacombe, M.; Peng, C. Y.; Ayala, P. Y.; Chen, W.; Wong, M. W.; Andres, J. L.; Replogle, E. S.; Gompertes, R.; Martin, R. L.; Fox, D. J.; Binkley, J. S.; Defrees, D. J.; Baker, J.; Stewart, J. P.; Head-Gordon, M.; Gonzalez, C.; Pople, J. A. *Gaussian 94*, Revision E.2; Gaussian, Inc.: Pittsburgh, PA, 1995.

(32) McDouall, J. J. W.; Peasley, K.; Robb, M. A. *Chem. Phys. Lett*. **1988**, *148*, 183.